Available online at www.sciencedirect.com
SCIENCE DIRECT®
Journal of Solid State Chemistry 177 (2004) 772–780
JOURNAL OF SOLID STATE CHEMISTRY
http://elsevier.com/locate/jssc

Synthesis and characterization of a novel nano-scale magnetic solid base catalyst involving a layered double hydroxide supported on a ferrite core ☆

Hui Zhang, Rong Qi, David G. Evans, and Xue Duan*

Ministry of Education Key Laboratory of Science and Technology of Controllable Chemical Reactions, Beijing University of Chemical Technology, Box 98, Beijing 100029, China

Received 9 July 2003; received in revised form 31 August 2003; accepted 7 September 2003

Abstract

A nano-scale magnetic solid base catalyst MgAl-OH-LDH/$MgFe_2O_4$ (where LDH denotes layered double hydroxide) composed of MgAl-OH-LDH Brønsted base catalytic layers coated on $MgFe_2O_4$ spinel cores has been prepared. A magnetic precursor MgAl-CO_3-LDH/$MgFe_2O_4$ was prepared by a method involving separate nucleation and aging steps, and subsequently calcined to give a mixed metal oxide composite MgAl(O)/$MgFe_2O_4$ which was rehydrated to give MgAl-OH-LDH/$MgFe_2O_4$. The structure and magnetic properties of the nano-scale magnetic solid base MgAl-OH-LDH/$MgFe_2O_4$, together with those of the magnetic precursor MgAl-CO_3-LDH/$MgFe_2O_4$ and $MgFe_2O_4$ were characterized by XRD, XPS, low temperature N_2 adsorption and vibrating sample magnetometry (VSM). The MgAl-OH-LDH/$MgFe_2O_4$ composite possesses a mesoporous structure with pore size ranging from 2 to 20 nm with particle size mainly in the range 35–130 nm. The catalytic properties of MgAl-OH-LDH/$MgFe_2O_4$ were evaluated using the self-condensation of acetone at 273 K as a probe reaction. The results showed that the conversion of acetone to diacetone alcohol reached the thermodynamic equilibrium value of 23% at 273 K. The catalyst was easily recovered through application of an external magnetic field, and when the reclaimed catalyst was used in a second run for the same reaction, the reactivity remained unchanged.

Keywords: Nano-scale; Magnetic core; Solid base; MgAl-OH-LDH/$MgFe_2O_4$; Aldol condensation; Acetone

1. Introduction

Layered double hydroxides (LDHs) are a class of promising solid base catalysts which have the general formula $[M(\mathrm{II})_{1-x}M(\mathrm{III})_x(\mathrm{OH})_2]^{x+}$ $(A^{n-})_{x/n}\cdot mH_2O$, where M(II) and M(III) are metal cations, $x = M(\mathrm{III})/\{M(\mathrm{III})+M(\mathrm{II})\}$ and A^{n-} denotes anions. The structure of LDHs consists of brucite-like layers, with M(II) cations partially substituted by M(III) cations resulting in a net positive charge which is compensated by interlayer anions in the hydrated interlayer region [1]. The basic properties of LDHs and materials derived from them can be tailored by altering the identity of the cations in the layers, the M(II)/M(III) ratio, the nature of the compensating anions, and the activation conditions [2]. The resulting materials are effective environmentally friendly solid base catalysts for reactions such as aldol condensations [3], alkylation [4] and isomerization [5]. Their high catalytic activities are related directly to their surface and textural properties, for example the very small or nanometer particle size, high surface areas, and shape and size distributions of pores. In general, the surface area of a catalyst increases with decreasing particle size, so that nanometer sized solid base particles should have more basic sites on the surface than larger particles, and thus have enhanced catalytic activity. For nanometer sized catalyst particles however, there are considerable difficulties in separating and reclaiming the catalyst at the end of the reaction in liquid systems. In order to overcome this problem, we have designed a magnetic nano-scale solid base catalyst, by combining a magnetic material with a solid base, which allows simple and effective reclamation of the catalyst at the end of the reaction by using an external magnetic field.

☆ Supported by National Natural Science Foundation of China (No. 20076003).
* Corresponding author. Fax: +8610-64425385.
E-mail address: duanx@mail.buct.edu.cn (X. Duan).

0022-4596/$ - see front matter © 2003 Elsevier Inc. All rights reserved.
doi:10.1016/j.jssc.2003.09.009

There have been some earlier reports in the literature of the use of magnetic separation in catalysis. Reetz et al. [6] incorporated a lipase and Fe_3O_4 in a hydrophobic sol–gel material to give catalytically active and magnetically separable heterogeneous biocatalysts. Beydoun et al. [7] synthesized magnetic photocatalysts by coating TiO_2 particles on Fe_3O_4 nano-magnetite particles in order to facilitate easy recovery by a magnetic field. The photocatalysts were used in water treatment, but their photoactivity was lower than that of single phase TiO_2 due to unfavorable heterojunctions between the titanium dioxide and the iron oxide core. Fomenko et al. [8] prepared new catalysts including α-Fe_2O_3 and a solid solution formed from magnetite and Mg-ferrite for oxidative conversion of methane followed by magnetic separation. In our laboratory, magnetic solid acid catalysts $Zr(SO_4)_2/Fe_3O_4$ involving a coated structure have been designed and used successfully [9,10]. However, because of the instability of Fe_3O_4 at high temperatures, magnetic solid base catalysts with magnesium ferrite ($MgFe_2O_4$) as the magnetic cores should have wider applicability. $MgFe_2O_4$, is a soft magnetic material, which has been widely investigated [11–14]. The traditional method for preparing bulk $MgFe_2O_4$ is a solid-state reaction involving mixing, grinding, and finally calcination of α-Fe_2O_3 and magnesia, usually requiring a long time. Furthermore, highly pure spinel products cannot be obtained, and the particles are always large in size. Nanosized ferrite materials can be synthesized by many methods, for instance, coprecipitation [15], sol–gel processes [16], and high-energy ball milling [17]. However, these methods result in ultrafine spinel ferrite powders, which display superparamagnetic properties at room temperature due to their tiny particle size, and ferromagnetic behavior is exhibited only at very low temperature. The superparamagnetic $MgFe_2O_4$ particles are not suitable for a magnetic catalyst core. In order to prepare a ferrite with particle size larger than 30 nm, we employed a new method [18–20] developed in our laboratory. The distinctive features of this method are a very rapid mixing and nucleation process followed by a separate aging step, which results in nanometer particles with a narrow range of particle size [20].

In this work, our method involving separate nucleation and aging steps was employed to prepare both the magnetic core $MgFe_2O_4$ and the magnetic catalyst precursor MgAl-CO_3-LDH/$MgFe_2O_4$. The latter was converted to the magnetic solid base catalyst MgAl-OH-LDH/$MgFe_2O_4$ by calcination followed by rehydration. The structural, textural and magnetic properties of the materials were examined. The catalytic activity of the catalyst was evaluated using the liquid-phase aldol condensation of acetone as a probe reaction.

2. Experimental

2.1. Synthesis

2.1.1. Synthesis of the magnetic core $MgFe_2O_4$

The magnetic core $MgFe_2O_4$ was prepared from an MgFe-LDH precursor synthesized using the method developed in our laboratory [18–20]. A typical synthesis is as follows: an aqueous solution of $Mg(NO_3)_2 \cdot 6H_2O$ and $Fe(NO_3)_3 \cdot 9H_2O$ with different Mg^{2+}/Fe^{3+} ratios and a second solution with pH ~ 9 containing NaOH and Na_2CO_3 in deionized water were simultaneously added to a colloid mill rotating at 4000 rpm and mixed for 2 min. The resulting slurry was removed from the reactor and aged at 373 K for 6 h. The final precipitate was filtered, washed thoroughly with deionized water and dried at 343 K for 24 h. The resulting sample was then calcined at 1173 K for 2 h, resulting in the $MgFe_2O_4$ magnetic core.

2.1.2. Synthesis of the magnetic catalyst precursor MgAl-CO_3-LDH/$MgFe_2O_4$

An aqueous solution of $Mg(NO_3)_2 \cdot 6H_2O$ and $Al(NO_3)_3 \cdot 9H_2O$ with an Mg^{2+}/Al^{3+} ratio of 3, and 1.6 g $MgFe_2O_4$ ($Mg^{2+}/MgFe_2O_4$ ratio of 2.4, by mass) were mixed to form a suspension. This mixture and a solution with pH ~ 11 containing NaOH and Na_2CO_3 in deionized water were simultaneously added to a colloid mill rotating at 4000 rpm and mixed for 2 min. The resulting slurry was removed from the reactor and aged at 373 K for 6 h. The precipitate was filtered, washed thoroughly with deionized water and dried at 343 K for 24 h, giving the magnetic precursor MgAl-CO_3-LDH/$MgFe_2O_4$.

2.1.3. Synthesis of the magnetic solid base catalyst MgAl-OH-LDH/$MgFe_2O_4$

MgAl-CO_3-LDH/$MgFe_2O_4$ was calcined at 773 K in air for 6 h with a initial heating rate of 5 K/min to produce a mixed metal oxide coating on the magnetic core, denoted as MgAl(O)/$MgFe_2O_4$. This powder was dispersed in decarbonated water (30 mL H_2O/g of MgAl(O)/$MgFe_2O_4$) with vigorous stirring for 1 h at 298 K under an N_2 atmosphere. The excess water was removed under vacuum at 323 K.

2.2. Characterization

Powder X-ray diffraction (XRD) patterns were obtained with a Rigaku XRD-6000 diffractometer under the following conditions: 40 kV, 30 mA, Cu$K\alpha$ radiation ($\lambda = 1.542$ Å), scan steps of 0.04°/min (10 s) in the range of 3–70°. Mössbauer spectra were obtained at room temperature using a conventional constant acceleration spectrometer. A radiation source of ^{57}Co in an Rh matrix was used. Elemental analysis was performed

by inductively coupled plasma emission spectroscopy (ICP) using a Shimadzu ICPS-7500 instrument. Low temperature N_2-adsorption measurements were recorded using a Quantachrome Autosorb-1 system. Samples were pretreated by heating at 383 K under vacuum for 2 h. Specific surface areas were calculated by the BET equation and pore size distributions were calculated from the desorption branch using the BJH method. The particle size distribution was determined using a Malvern Mastersizer 2000 laser particle size analyzer. Magnetic properties of the samples were studied by using a JSM-13 Vibrating Sample Magnetometer with a magnetic field of 12000 Oe. Scanning electron micrographs (SEM) were observed on a Cambridge S-250 MK3 instrument. Transmission electron micrographs (TEM) were recorded on a Hitachi-800 electron microscope. The samples were dispersed in ethanol and then treated ultrasonically in order to disperse individual particles over a copper grid. Surface chemical composition was studied by X-ray photoelectron spectroscopy (XPS) using a VG ESCA-LAB-220I-XL X-ray photoelectron spectrometer. The pressure in the analysis chamber during the experiments was 3×10^{-9} mbar. Spectra were acquired using a standard Al$K\alpha$ source ($h\nu = 1486.6$ eV) operating at 15 kV and 20 mA. The binding energy scale was referenced to the C1 s line of aliphatic carbon contamination set at 284.6 eV.

2.3. Evaluation of the magnetic nano-scale solid base catalyst

Catalytic activity of the solid bases was evaluated using the liquid-phase aldol condensation of acetone (>99.9%; Aldrich) as a probe reaction. The reaction was carried out at 273 K under an N_2 atmosphere in a well-agitated 250 mL round bottomed flask maintained in an ice bath. Typically, 2 wt% of the catalyst relative to acetone was used. The mixture of products was analyzed by gas chromatography. Conversion to diacetone alcohol (DAA) was monitored as a function of reaction time. After one reaction run, the mixture of reactants, products and magnetic catalyst was transferred to a beaker equipped with an external magnetic field of 385 G. The magnetic catalyst was attracted to the bottom of the beaker. Liquid was easily removed, and the catalyst was reclaimed for the next run.

3. Results and discussion

3.1. Structure and properties of the magnetic core $MgFe_2O_4$

3.1.1. XRD characterization

The XRD patterns of MgFe-LDHs, i.e. the precursors of the magnetic core, and their calcined products are shown in Fig. 1A and B. It can be seen that all three precursors have the characteristic structure of hydrotalcite-like compounds [1,21,22]. The MgFe-LDH with an Mg/Fe ratio of 1:2 shows poorer crystallinity than those having Mg/Fe ratios of 2:1 and 1:1, due to the higher charge density in the layers [1,21]. However, this sample gives more crystalline $MgFe_2O_4$ on calcination, with smaller amounts of iron oxides than other samples. As shown in Fig. 1B, after calcining at 1173 K, the characteristic reflection peaks of the MgFe-LDHs disappear and new phases are formed. Five strong peaks located at 30.2°, 35.5°, 43.2°, 57.0° and 62.7°, and two weak peaks at 37.1° and 53.6° are observed in the XRD patterns of the calcined samples, which can be assigned to the (220), (311), (400), (511), (440), (222) and (422) reflections, respectively, of the $MgFe_2O_4$ spinel structure (JCPDS 17-0465). The characteristic reflections of MgO at 43.2° and 62.7° overlap with the spinel (400) and (440) reflections, but from the relative intensity of the peaks, it is possible to estimate the

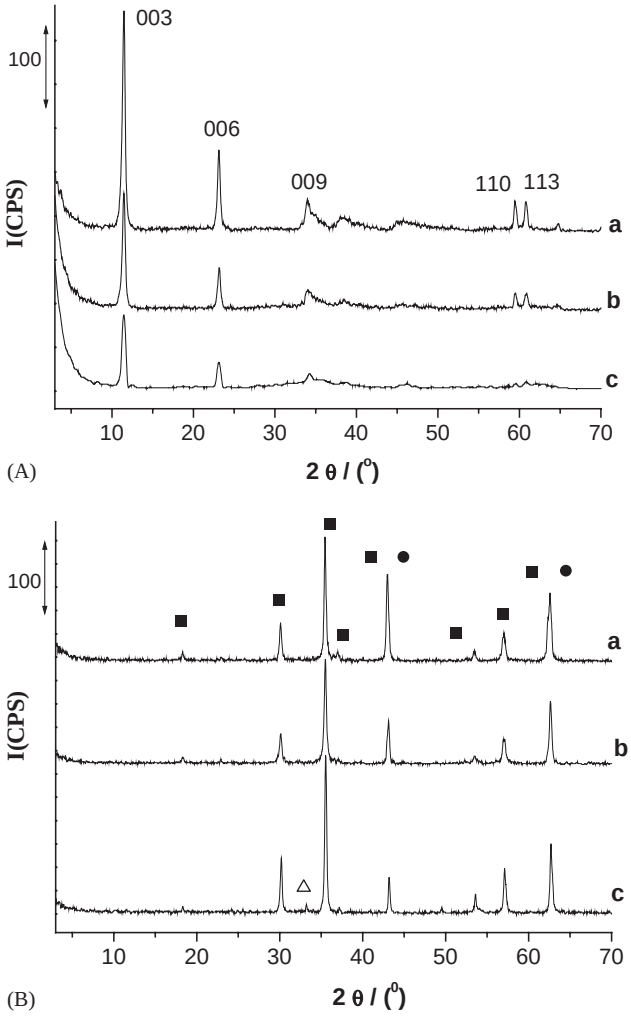

Fig. 1. XRD patterns of MgFe-LDH with various Mg/Fe ratios (A) and samples calcined at 1173 K (B). (a) 2:1, (b) 1:1, (c) 1:2, ●MgO; ■$MgFe_2O_4$; △α-Fe_2O_3.

different amounts of MgO. The characteristic reflections of α-Fe_2O_3 at 33.2° and 49.5° can also be seen in Fig. 1B(c). Taking into account both the relative intensity and width of the reflections in Fig. 1B, it can be seen that the spinel with the highest crystallinity was obtained from the MgFe-LDH having an Mg/Fe ratio of 1:2, and this calcined sample was employed as the magnetic core in our work.

3.1.2. Mössbauer spectroscopy

Fig. 2 shows the room temperature Mössbauer spectrum of the $MgFe_2O_4$ sample. $MgFe_2O_4$ displays an asymmetrical sextet that is characteristic of the presence of a magnetic hyperfine field distribution [23]. Deconvolution showed that this hyperfine six-line spectrum can be fitted by three six-line sub-spectra (also shown in Fig. 2) whose calculated parameters are summarized in Table 1, suggesting that three different Fe species are present in the sample. According to the values of the isomer shifts, the iron is exclusively in oxidation state +3 since the isomer shifts δ are less than 0.54 mm s^{-1} [24]. Two of the six-line sub-spectra can be ascribed to Fe^{3+} at A- and B-sites in the $MgFe_2O_4$ spinel. The isomer shift of Fe^{3+} at B-sites (0.253 mm s^{-1}) is less than that at A-sites (0.326 mm s^{-1}) due to the difference in Fe^{3+}–O^{2-} internuclear separations [24]. From the relative areas of the sub-spectra peaks, the amount of Fe^{3+} at B-sites is greater than that at A-sites. The quadrupole splitting (ΔE) data give further insight into the cubic spinel structure. The larger the absolute value of ΔE, the greater the deviation of local symmetry from cubic symmetry, that is, Fe^{3+} ions at A-sites (27.7%) with quadrupole splitting of 0.023 mm s^{-1} are in slightly more distorted cubic symmetry compared with those at B-sites (0.007 mm s^{-1}) [24]. The hyperfine field corresponding to the third six-line sub-spectrum is 51.6 T, demonstrating [24] the existence of α-Fe_2O_3 in the sample with a content of merely 6.6%, in agreement with XRD analysis.

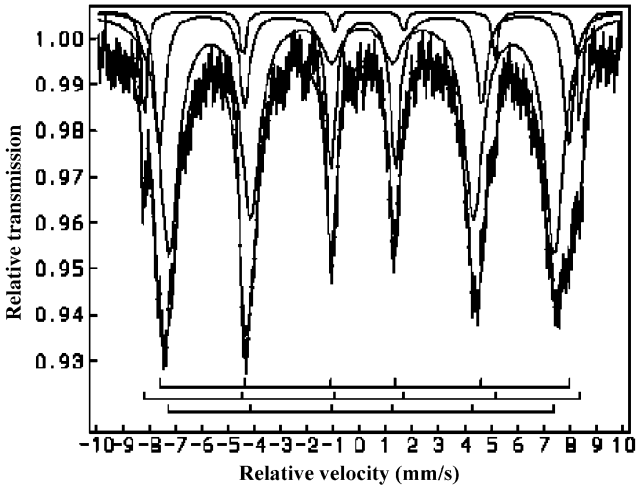

Fig. 2. Room temperature Mössbauer spectrum of $MgFe_2O_4$. The hyperfine six-line spectrum can be fitted with the three groups of six-line sub-spectra shown in the figure, suggesting that three different Fe species are present in the sample.

3.1.3. Magnetic properties, specific surface area and particle size

When the magnetization of the $MgFe_2O_4$ core material was measured as a function of the applied field at room temperature, the characteristic [25] hysteresis loop shown in Fig. 3a was obtained. The measured

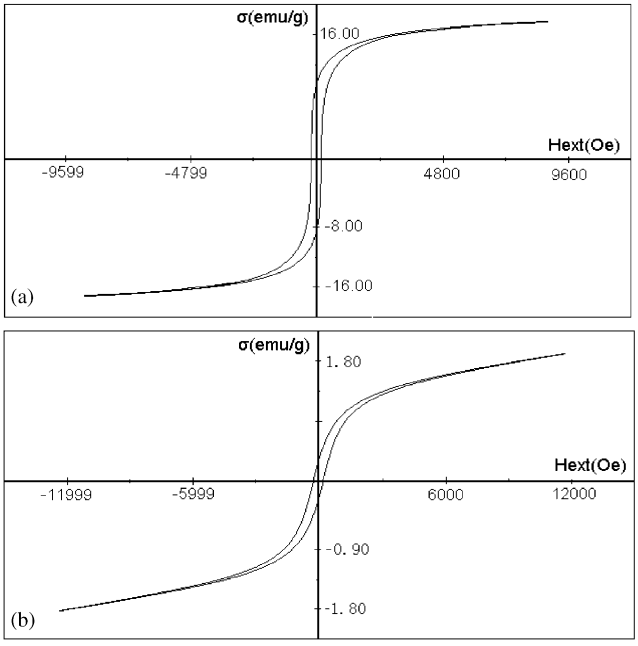

Fig. 3. Variation in magnetization (in emu/g) of (a) $MgFe_2O_4$ and (b) MgAl-OH-LDH/$MgFe_2O_4$ at room temperature as a function of the applied field (in Oe). The observed hysteresis loops are characteristic of soft ferromagnetic materials.

Table 1
Mössbauer spectral data of $MgFe_2O_4$ at room temperature IS (mm s^{-1}): isomer shift relative to sodium nitroprusside; ΔE (mm s^{-1}): quadrupole splitting

Iron species	FWHM/mm s^{-1}	IS/mm s^{-1}	ΔE /mm s^{-1}	Spectral contribution/%
Fe^{3+}(A)	0.453±0.052	0.326±0.017	0.023±0.009	27.71
Fe^{3+}(B)	0.855±0.039	0.253±0.017	−0.007±0.008	65.68
Fe_2O_3	0.228±0.034	0.393±0.017	−0.134±0.013	6.61

saturation magnetization intensity σ_s was 18.40 emu/g, indicative of strong soft magnetic properties [25]. Low temperature N_2 adsorption–desorption measurements gave a specific surface area of only 5.4 $m^2 g^{-1}$. Laser particle size analysis showed that uniform nano-scale $MgFe_2O_4$ particles with diameters around 60 nm had been prepared.

3.2. Structure of the magnetic catalyst precursor MgAl-CO_3-LDH/$MgFe_2O_4$

The XRD pattern of MgAl-CO_3-LDH/$MgFe_2O_4$ is illustrated in Fig. 4a. The presence of the hydrotalcite-like compound is clearly demonstrated. The three peaks at low 2θ angles correspond to the basal reflection and higher order reflections, and the two peaks at $2\theta \sim 60°$ are due to the (110) and (113) reflections [1]. The high relative intensity and symmetry of these peaks confirm the good crystallinity of the layered phase. At the same time, the characteristic reflections of $MgFe_2O_4$ can be observed at 2θ angles of 30.2°, 35.5°, 43.2°, 57.0° and 62.7° with lower intensity, due to its relatively low content. This suggests the presence of $MgFe_2O_4$ cores does not influence the formation of crystalline MgAl-CO_3-LDH and the two phases maintain their structural integrity in the composite magnetic catalyst precursor MgAl-CO_3-LDH/$MgFe_2O_4$.

The TEM micrograph of MgAl-CO_3-LDH/$MgFe_2O_4$ (Fig. 5a) shows the regular hexagonal morphology characteristic of hydrotalcite-like materials. After calcination at 773 K, MgAl-CO_3-LDH/$MgFe_2O_4$ is converted into MgAl(O)/$MgFe_2O_4$ by a process involving decomposition of the interlayer carbonate anions. The XRD pattern of MgAl(O)/$MgFe_2O_4$ (Fig. 4b) shows the complete disappearance of the (00*l*) reflections of the

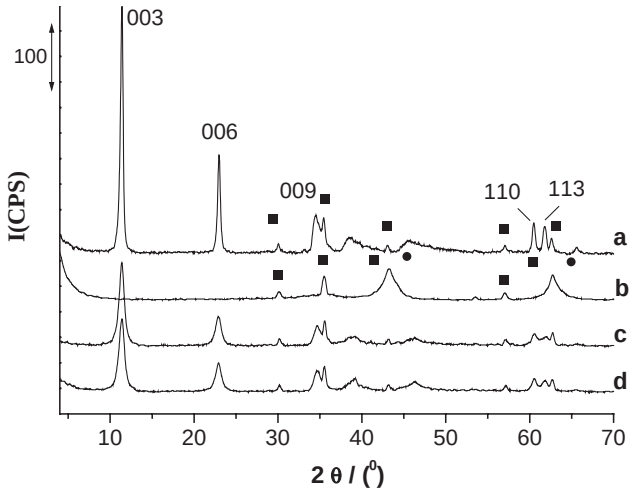

Fig. 4. XRD patterns of magnetic precursor MgAl-CO_3-LDH/$MgFe_2O_4$ (a), calcined product MgAl(O)/$MgFe_2O_4$ (b), magnetic solid base catalyst MgAl-OH-LDH/$MgFe_2O_4$ (c) and reclaimed magnetic solid base catalyst (d) (●, MgO; ■, $MgFe_2O_4$).

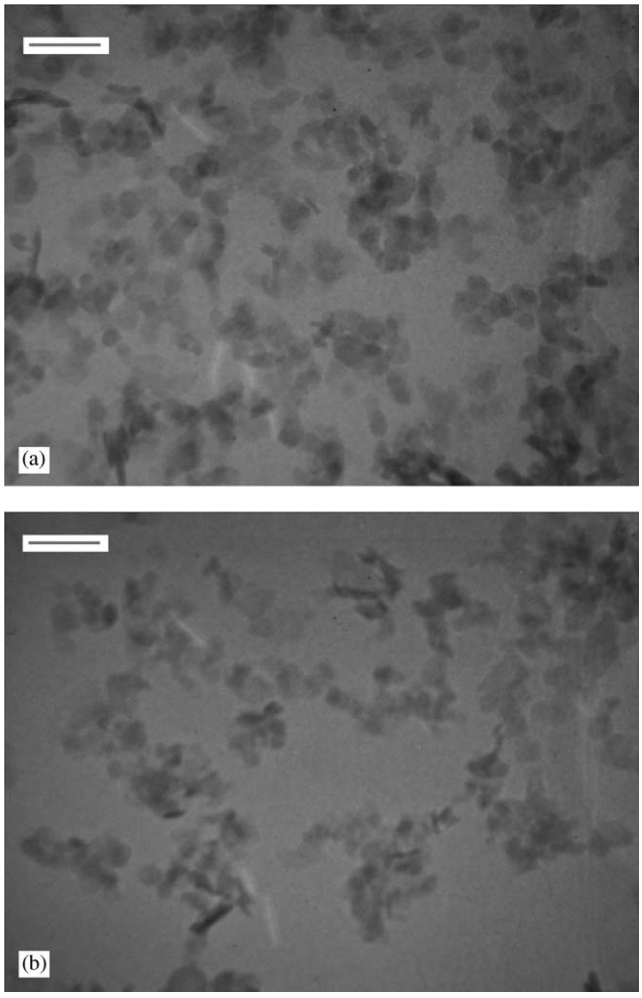

Fig. 5. TEM micrographs of (a) MgAl-CO_3-LDH/$MgFe_2O_4$ and (b) MgAl(O)/$MgFe_2O_4$ (Scale bar = 200 nm in both cases).

LDH structure and the appearance of the characteristic reflections [1] of a mixed oxide denoted as MgAl(O) at 2θ values of 43.3° and 62.6°. Meanwhile the characteristic diffraction pattern of $MgFe_2O_4$ remains unchanged although the (400) and (440) reflections are overlapped by the broad peaks due to MgAl(O).

The TEM micrograph of MgAl(O)/$MgFe_2O_4$ (Fig. 5b) shows that the morphology of the mixed LDH phase is essentially retained on calcination, although the hexagonal crystals become slightly less regular in shape.

3.3. Structure and properties of magnetic solid base MgAl-OH-LDH/$MgFe_2O_4$

3.3.1. Crystal structure and morphology

The XRD pattern of the magnetic solid base catalyst MgAl-OH-LDH/$MgFe_2O_4$ produced by rehydration of MgAl(O)/$MgFe_2O_4$ is shown in Fig. 4c. The appearance of new peaks characteristic of the layered structure of LDH and the disappearance of the MgAl(O) reflections can be clearly observed. The comparatively broad (00*l*)

reflections and a d_{003} spacing of 0.77 nm, are in good agreement with the literature for an LDH which has a meixnerite-like structure containing interlayer hydroxide ions and a small crystallite size [26]. The asymmetric broadening of the (110) and (113) reflections is indicative of a turbostratic disorder which alters the shape of all (*hk*0) reflections [27]. Furthermore, the characteristic reflections of $MgFe_2O_4$ are unchanged, indicating that the reconstruction procedure does not perturb the structure of $MgFe_2O_4$.

SEM and TEM micrographs of MgAl-OH-LDH/$MgFe_2O_4$ are shown in Fig. 6. The SEM micrograph (Fig. 6a) illustrates that the particles are covered with a network of thin plates, leading to micro-sized sponge-like aggregates, which is very similar to regenerated LDHs with CO_3^{2-} anions in the interlayer [28]. The TEM micrograph (Fig. 6b) clearly demonstrates the presence of irregular hexagonal plate-like particles with diameters in the range 50–100 nm. A high-resolution TEM micrograph (Fig. 6c) clearly reveals the presence of a ferrite core coated with a thin layer of the LDH material.

3.3.2. Magnetic properties and particle size

When the magnetization of MgAl-OH-LDH/$MgFe_2O_4$ was measured as a function of the applied field at room temperature, the characteristic [25] hysteresis loop shown in Fig. 3b was obtained. The measured saturation magnetization intensity σ_s was only 1.80 emu/g, much lower than that of the $MgFe_2O_4$ core material alone. Although this σ_s value is relatively low, it is still possible for magnetic separation of catalyst from the reactants by application of an appropriate external magnetic field. The reduction in the σ_s value of MgAl-OH-LDH/$MgFe_2O_4$ compared with that of $MgFe_2O_4$ is consistent with the lower content of the spinel phase in MgAl-OH-LDH/$MgFe_2O_4$. Indeed, our experiments with different loadings of MgAl-LDH on $MgFe_2O_4$ confirm that the saturation magnetization decreases with increasing MgAl-LDH loading.

Laser particle size analysis of MgAl-OH-LDH/$MgFe_2O_4$ gave a narrow particle size distribution in the range 35–130 nm, which is in good agreement with the TEM results.

3.3.3. Surface area and pore structure

The low temperature N_2 adsorption and desorption isotherms of MgAl-OH-LDH/$MgFe_2O_4$ are shown in Fig. 7. A type IV isotherm with a broad hysteresis loop is observed in the middle range of relative pressure, typical of mesoporous solids [29]. At low relative pressure ($p/p_0 < 0.3$) the prevailing process is the formation of a monolayer, while multilayer adsorption takes place at a higher relative pressure. At $p/p_0 > 0.3$ capillary condensation occurs in the mesopores, resulting in a gradual small increase in N_2 adsorption.

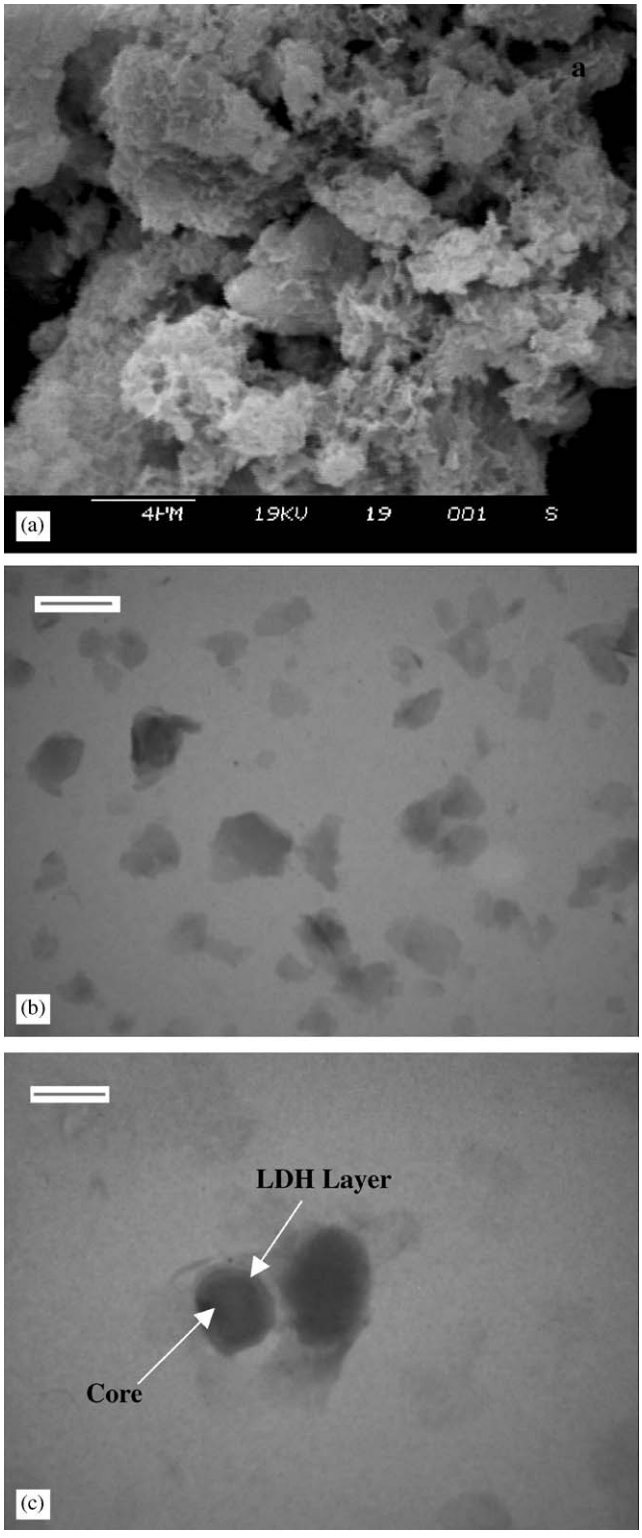

Fig. 6. SEM (a) (Scale bar = 4000 nm) and TEM {(b) Scale bar = 200 nm, (c) Scale bar = 67 nm} micrographs of MgAl-OH-LDH/$MgFe_2O_4$.

However, at $p/p_0 > 0.85$, the adsorption isotherm rises abruptly due to capillary condensation in large mesopores and macropores. The form of the hysteresis loop is

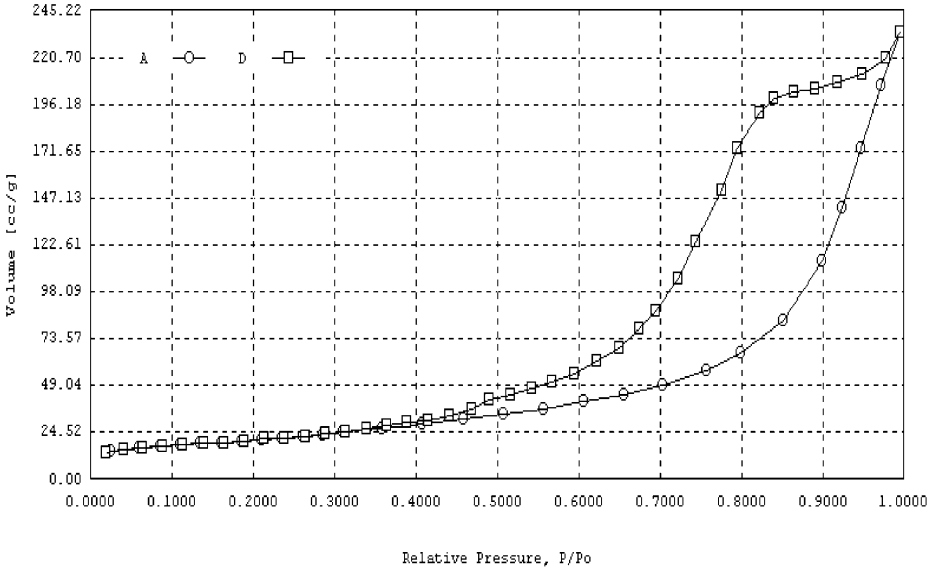

Fig. 7. N_2 adsorption–desorption isotherms of MgAl-OH-LDH/$MgFe_2O_4$.

a combination of types H2 and H4 (predominantly H2, probably) according to the IUPAC classification [30], suggesting that these pores are mainly slit-like or groove-like in shape, which might be related to the randomly stacked layered structure of the MgAl-OH-LDH/$MgFe_2O_4$. The irregular form of the hysteresis loop also indicates the presence of non-uniformity in pore size and/or shape. The pore size of MgAl-OH-LDH/$MgFe_2O_4$ is in the range 2–20 nm with a small fraction of macropores. The BET specific surface area is $77\,m^2\,g^{-1}$. The magnetic solid base MgAl-OH-LDH/$MgFe_2O_4$ has a mesoporous structure and reasonably high surface area, which should prove beneficial in catalytic reactions.

3.3.4. XPS analysis

In order to investigate the microstructure of MgAl-OH-LDH/$MgFe_2O_4$ and the interaction between $MgFe_2O_4$ and MgAl-OH-LDH phases, the surface chemical composition was determined by XPS analysis. For comparison, XPS data for $MgFe_2O_4$ and MgAl-OH-LDH together with ICP analysis are given in Table 2. It can be seen that the detectable elements on the surface of MgAl-OH-LDH/$MgFe_2O_4$ are Mg, Al, Fe and O with atom percentages of 33.69%, 8.63%, 0.09% and 57.59%, respectively. The signal for Fe is very weak, and the Mg/Fe ratio on the surface is calculated to be 387, which is much greater than the bulk composition of MgAl-OH-LDH/$MgFe_2O_4$ on the basis of ICP analysis. This shows that the Fe^{3+} is predominantly located in the interior rather than on the surface, confirming that the MgAl-OH-LDH phase exists as a surface layer and $MgFe_2O_4$ is embedded in the core of the composite material.

Table 2
XPS and ICP data

	Binding energy/eV				
	Mg2p	Al2p	$Fe2p_{3/2}$	O1s	C1s
MgAl-OH-LDH/$MgFe_2O_4$	49.4	73.9	710.8	531.4	284.6
$MgFe_2O_4$	48.8	—	710.9	529.9	284.6
MgAl-OH-LDH	49.4	73.9	—	531.4	284.6
MgAl-OH-LDH/$MgFe_2O_4$	Surface[a]		Bulk[b]		
Mg/Fe (mol/mol)	387		10.3		
Mg/Al (mol/mol)	3.92		2.17		

[a] Based on XPS data.
[b] Based on ICP data.

Binding energies are not only element specific, but also contain chemical information, because the energy levels of core electrons depend on the chemical state of the atom. Chemical shifts arise from the variation of electrostatic screening experienced by core electrons, as valence electrons are drawn towards or away from the atom [31]. From Table 2, it can be seen that the binding energies of Mg2p, Al2p, and O1s in MgAl-OH-LDH/$MgFe_2O_4$ are same as those in MgAl-OH-LDH, confirming the presence of the MgAl-OH-LDH layers in the composite. However, for MgAl-OH-LDH/$MgFe_2O_4$, the binding energy of $Fe2p_{3/2}$ is slightly lower than that for $MgFe_2O_4$, while the binding energy of O1s of MgAl-OH-LDH/$MgFe_2O_4$ is higher than that for $MgFe_2O_4$. Although small, these shifts are consistent with an interaction between the MgAl-OH-LDH phase and the magnetic core $MgFe_2O_4$ through Mg–O–Fe and Al–O–Fe bonds formed at the interface. Given that the electronegativity of Fe is higher than that of Mg and Al, the electron density at Fe^{3+} increases as Fe^{3+} is linked

with Mg^{2+} or Al^{3+} through oxygen atoms, inducing a stronger electrostatic shielding for Fe^{3+}. The binding energy thus decreases for $Fe2p_{3/2}$, whereas it increases for O1s.

On the basis of the above analysis, we propose a tentative model for the magnetic solid base MgAl-OH-LDH/$MgFe_2O_4$ catalyst as shown in Fig. 8. The structure involves MgAl-OH-LDH Brønsted base catalytic layers supported on $MgFe_2O_4$ spinel cores through Mg–O–Fe and Al–O–Fe linkages. Not only are the structures of MgAl-OH-LDH and $MgFe_2O_4$ maintained, but the catalytically active OH^- sites are also exposed on the particle surface, which should be favorable for base-catalyzed reactions.

3.3.5. Catalytic activity

The aldol condensation of acetone is often used as a model system for fundamental studies of the catalytic properties of LDHs [3,26,32]. The main product obtained is diacetone alcohol (DAA), with a small amount of mesityl oxide formed by dehydration [26].

The catalytic activity of the magnetic solid base MgAl-OH-LDH/$MgFe_2O_4$ was tested in the aldol condensation of acetone, together with MgO, $Mg(OH)_2$ and the magnetic material $MgFe_2O_4$ alone for comparison. Fig. 9 shows the catalytic performance of these materials. $Mg(OH)_2$ and $MgFe_2O_4$ samples are catalytically inactive and MgO gives very low DAA conversion (only 0.68% after 265 min). This is due to their lack of surface Brønsted base sites, which are the catalytically

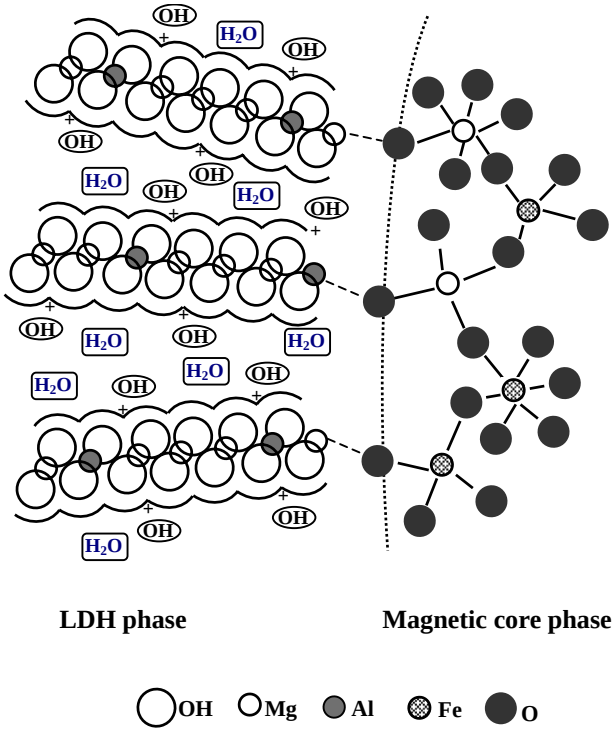

Fig. 8. Structural model of MgAl-OH-LDH/$MgFe_2O_4$.

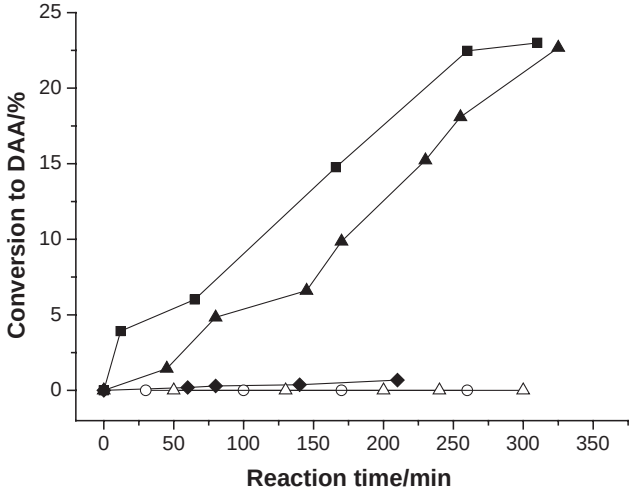

Fig. 9. Activity of different catalysts in the aldol condensation of acetone: DAA conversion as a function of reaction time (■, fresh MgAl-OH-LDH/$MgFe_2O_4$; ▲, recovered MgAl-OH-LDH/$MgFe_2O_4$; ♦, MgO; ○, $Mg(OH)_2$; △, $MgFe_2O_4$).

active centers for the aldol condensation of acetone [3,26]. In contrast however, MgAl-OH-LDH/$MgFe_2O_4$ has very high catalytic activity and selectivity to DAA. The DAA conversion increases with reaction time, and after 310 min reaches 23%, which is very close to the thermodynamic equilibrium conversion (23.1%) at 273 K [3]. This value is higher than that reported in the literature [26] for unsupported MgAl-OH-LDH.

The higher catalytic activity of MgAl-OH-LDH/$MgFe_2O_4$ compared with that of MgAl-OH-LDH indicates that the introduction of the magnetic material $MgFe_2O_4$ not only does not reduce catalytic activity, in fact it slightly promotes the conversion to DAA. According to the literature [26], only OH^- ions near edges of platelets are effective in catalyzing the aldol condensation. It is reasonable to assume that a larger number of basic OH^- sites occur on the surface layers of MgAl-OH-LDH/$MgFe_2O_4$ compared with bulk MgAl-OH-LDH. In the synthesis process of the magnetic precursor MgAl-CO_3-LDH/$MgFe_2O_4$ as well as subsequent calcination and rehydration steps, the magnetic cores $MgFe_2O_4$ become well dispersed, supporting MgAl-OH-LDH as surface layers, thus reducing aggregation of particles, leading to the irregular plate-like layered structure revealed by TEM in Fig. 6(b). In this way, MgAl-OH-LDH/$MgFe_2O_4$ has more OH^- sites exposed on the surface layers than bulk MgAl-OH-LDH, and exhibits higher activity.

After one run in the aldol condensation of acetone, the nano-scale magnetic catalyst MgAl-OH-LDH/$MgFe_2O_4$ was reclaimed by application of an external magnetic field of 385 G with a reclaim ratio of 86 wt%, and then used in second run. The DAA conversion over reclaimed MgAl-OH-LDH/$MgFe_2O_4$ as a function of

time is also shown in Fig. 9. It can be seen that high activity, comparable to that of fresh sample, was obtained for DAA conversion (up to 22.7% after 325 min of reaction). The weight loss of the catalyst can be attributed to some of the water molecules located in the interlayer region being removed with volatile acetone. Furthermore, the XRD pattern of the reclaimed catalyst shown in Fig. 4d is unchanged after reaction, which is consistent with the catalytic results.

4. Conclusions

A novel magnetic nano-scale solid base MgAl-OH-LDH/$MgFe_2O_4$ was synthesized from a layered precursor followed by calcination and rehydration steps. The MgAl-OH-LDH Brønsted base catalytic layers are coated over magnetic $MgFe_2O_4$ spinel cores, probably through Mg–O–Fe and Al–O–Fe linkages. This structure leads to a high activity of the synthesized MgAl-OH-LDH/$MgFe_2O_4$ in the aldol condensation of acetone, followed by effective reclamation through application of an external magnetic field. Introducing magnetic properties into nano-scale solid bases derived from layered double hydroxides by introducing magnetic cores may offer broad perspectives in tailoring the catalytic properties of these materials and easy recovery of the catalysts offers many potential applications.

References

[1] F. Cavani, F. Trifiro, A. Vaccari, Catal. Today 11 (1991) 173.
[2] D.J. Cosimo, V.K. Diez, M. Xu, E. Iglesia, C.R. Apesteguia, J. Catal. 178 (1998) 499.
[3] D. Tichit, M.N. Bennani, F. Figueras, R. Tessier, J. Kervennal, Appl. Clay Sci. 13 (1998) 401.
[4] W.T. Reichle, J. Catal. 94 (1985) 547.
[5] S. Velu, C.S. Swamy, Appl. Catal. 119 (1994) 241.
[6] M.T. Reetz, A. Zonta, V. Vijayakrishnan, K. Schimossek, J. Mol. Catal. A 134 (1998) 259.
[7] D. Beydoun, R. Amal, G.K.C. Low, S. McEvoy, J. Phys. Chem. B 104 (2000) 4387.
[8] E.V. Fomenko, E.V. Kondratenko, A.N. Salanov, Catal. Today 42 (1998) 267.
[9] Z. Chang, F. Li, X. Duan, Chin. J. Inorg. Chem. 17 (2001) 366.
[10] Z. Chang, C. Guo, F. Li, X. Duan, Acta Chim. Sinica 60 (2002) 298.
[11] V. Šepelák, D. Baabe, F.J. Litterst, K.D. Becker, Hyperfine Interactions. 126 (2000) 143.
[12] Z. Wang, P. Lazor, S.K. Saxena, H.St.C. O'Neill, Mater. Res. Bull. 37 (2002) 1589.
[13] V. Šepelák, D. Baabe, D. Mienert, F.J. Litterst, K.D. Becker, Scripta Mater. 48 (2003) 961.
[14] S.F. Moustafa, M.B. Morsi, Mater. Lett. 34 (1998) 241.
[15] Q. Chen, A.J. Rondinone, B.C. Chakoumakos, Z.J. Zhang, J. Magn. Magn. Mater. 194 (1999) 1.
[16] S.A. Oliver, R.J. Willey, H.H. Hamdeh, G. Oliveri, G. Busca, Scripta Metall. Mater. 33 (1995) 1695.
[17] V. Šepelák, D. Schultze, F. Krumeich, U. Steinike, K.D. Becker, Solid State Ionics 141–142 (2001) 667.
[18] X. Duan, Q.Z. Jiao, L. Li, Chinese Patent CN 99119385.7.
[19] X. Duan, Q.Z. Jiao, Chinese Patent CN 00132145.5.
[20] Y. Zhao, F. Li, R. Zhang, D.G. Evans, X. Duan, Chem. Mater. 14 (2002) 4286.
[21] J.-Y. Shen, B. Guang, M. Tu, Y. Chen, Catal. Today 30 (1996) 77.
[22] T. Hibino, A. Tsunashima, J. Mater. Sci. Lett. 19 (2000) 1403.
[23] G.M. Da Costa, E. De Grave, L.H. Bowen, P.M.A. De Bakker, R.E. Vandenberghe, Clays Clay Miner. 43 (1995) 562.
[24] H.St.C. O'Neill, H. Annersten, D. Virgo, Amer. Mineral. 77 (1992) 725.
[25] S.J. Blundell, Magnetism in Condensed Matter, Oxford University Press, New York, 2001, pp. 131–136.
[26] J.C.A.A. Roelofs, D.J. Lensveld, A.J. van Dillen, K.P. de Jong, J. Catal. 203 (2001) 184.
[27] M. Rajamathi, G.D. Nataraja, S. Ananthamurthy, P.V. Kamath, J. Mater. Chem. 10 (2000) 2754.
[28] T.S. Stanimirova, G. Korov, E. Dinolova, J. Mater. Sci. Lett. 20 (2001) 453.
[29] S.J. Gregg, K.S.W. Sing, Adsorption, Surface Area and Porosity, Academic Press, New York, 1982.
[30] K.S.W. Sing, D.H. Everett, R.A.W. Haul, L. Moscou, R.A. Pierotti, J. Rouquerol, T. Iemieniewska, Pure Appl. Chem. 57 (1985) 603.
[31] J.M. Walls, Methods of Surface Analysis, Cambridge University Press, Cambridge, 1989.
[32] F. Prinetto, D. Tichit, R. Teissier, B. Coq, Catal. Today 55 (2000) 103.